Inorganic Chemistry

Article

pubs.acs.org/IC

Elucidating Self-Assembly Mechanisms of Uranyl–Peroxide Capsules from Monomers

Zuolei Liao, Tapash Deb, and May Nyman*

Energy Frontier Research Center, Materials Science of Actinides Department of Chemistry, Oregon State University, Gilbert Hall, Corvallis, Oregon 97331, United States

Supporting Information

ABSTRACT: Self-assembly of uranyl peroxide polyoxometalates (POMs) in alkaline peroxide solutions has been known for almost a decade, but in these dynamic solutions that contain high concentrations of base and peroxide the reaction pathway could never be discerned, mixed species are obtained, and reproducibility is sometimes a challenge. Here we elucidate the reaction mechanisms utilizing self-assembly of the U_{24} cluster, $[UO_2(O_2)(OH)]_{24}^{24-}$, from monomers as a model system. Using Raman as our main spectroscopic probe, we learned that the monomeric species is persistent in water at room temperature indefinitely. However, if a redox-active transition metal catalyst (copper (Cu^{2+}) or cobalt (Co^{2+})) is added, self-assembly is accelerated in a significant manner, forming U_{24} peroxide clusters in several hours, which is a good time scale for studying reaction mechanisms. From semiquantitative treatment of the spectroscopic data, we elucidate reaction mechanisms that are consistent with prior structural and computational studies that suggest uranyl peroxide rings templated by alkalis are the building units of clusters. By understanding aqueous speciation and processes, we are moving toward assuming control over cluster self-assembly that has been mastered for decades now in the analogous transition-metal POM systems.

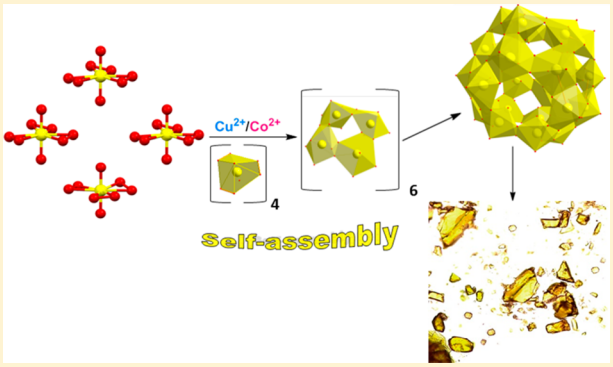

INTRODUCTION

Uranyl peroxide clusters have been known for almost a decade now,[1] and continued synthetic efforts have produced new structures with a huge range of topologies and sizes.[2−4] Despite the diversity in cluster geometries, most of the syntheses are the same: uranyl nitrate, excess peroxide, and base along with other ancillary ligands or heterometals are mixed together in a vial, followed by slow evaporation of solvent until crystals are harvested, typically with a time span of several days to several weeks.[1,5,6] The result often engenders low yield, irreproducibility, and a mixture of products. As an alternative route, uranyl triperoxide monomers are synthesized, isolated, and then redissolved in water to self-assemble into uranyl clusters.[7−9] Different uranyl peroxide cluster geometries could be obtained by guiding the self-assembly reaction using various directional counterions,[7,8,10−14] thus gaining some control obtaining pure-phase, targeted products. The latter approach revealed the possibility of the uranyl triperoxide monomers to be an intermediate species cluster formation in all self-assembly processes. In order to drive the reaction from uranyl triperoxide monomers toward clusters, excessive peroxide species must be released as (O_2) or converted to O^{2-} or OH^- via oxidation, reduction, and/or disproportionation. Therefore, it could be hypothesized that a catalyst capable of decomposing peroxide would have the potential to promote cluster formation.

One of the major potential applications for uranyl–peroxide clusters is isolating and recycling uranium from spent nuclear fuels.[15] However, with the presence of all of the fission products and supporting components of fabricated fuel pellets, the composition would be more complex than the relatively well-constrained syntheses performed in the laboratory. Reactions between uranyl peroxide species and ions/elements present in nuclear fuel reprocessing solutions are inevitable but far less studied. In particular, considering that peroxide can serve as an oxidizing or a reducing agent, it would very likely participate in and even induce side reactions. Additionally, studtite, the only naturally occurring peroxide mineral,[16] is believed to be formed by alpha-radiolysis of water. Studtite was also reported[17] to be formed on spent nuclear fuel and on the nuclear material ("lava") floating after the Chernobyl accident.[18] Both nature and nuclear reactors provide such "dirty" environments with many chemical impurities that inevitably would influence the reactivity of uranyl peroxide species. Therefore, to develop a fundamental understanding of the evolution, from uranyl peroxide monomers to polynuclear species, we need to begin to investigate the multitude of possible reactions that could occur.

Received: July 3, 2014
Published: September 19, 2014

As one such controlled study, we report here the effect of first-row transition metals on the evolution of uranyl peroxide monomers to clusters. Systematic studies to understand the effect of parameters such as uranyl and peroxide concentration require a carefully controlled system. The lithium $[UO_2(O_2)_3]^{4-}$ monomer is the optimal choice of all of the alkali monomers, based on its stability and solubility.[19] Moreover, it reliably and reproducibly forms $[UO_2(O_2)(OH)]_{24}^{24-}$ (also known as U_{24}) clusters, presumably due to the strong templating capability of Li^+ for the square faces that define this cluster. Briefly, U_{24} contains 24 $[U(O_2)_2(OH)_2]$ monomeric units that are linked into 6 square faces of 4 uranyls each. These are bridged with peroxide ligands within the square face. The square faces are linked together into hexagonal faces (total of 8 in U_{24}) through the hydroxyl ligands, and the uranyl nodes of the hexagonal faces are alternately joined by bridging peroxide ligands and two bridging hydroxyl ligands; see Figure 1. Finally, with Li^+ as the only alkali cation present, the polynuclear species that form (such as U_{24}) are highly soluble, whereas the heavier alkalis result in precipitation of the polymerizing species.

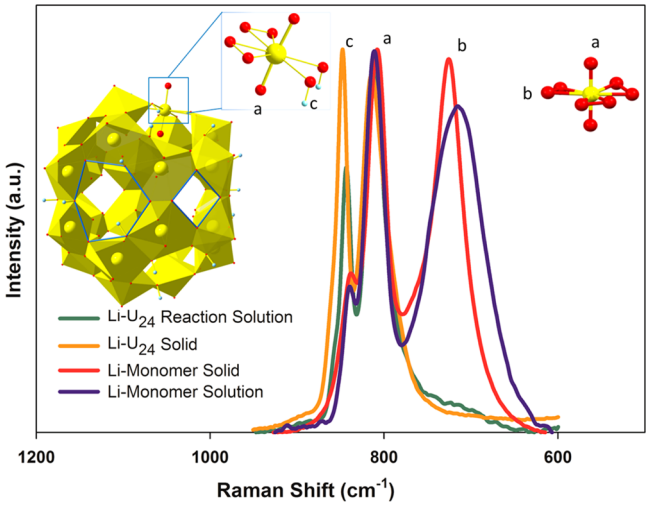

Figure 1. Raman spectra of Li monomer and Li–U_{24} in the solid state and aqueous solution. Uranyl (a), peroxide (b), and hydroxyl (c) peaks are shown in addition to hexagonal and square faces (highlighted in blue) on the U_{24} cluster (color code: H atoms = light blue, O atoms = red, U atoms = yellow).

Small-angle X-ray scattering (SAXS) and electrospray ionization mass spectroscopy (ESI-MS)[20] are useful to both fingerprint cluster species in solution and follow the growth of complex clusters from known skeleton structures.[21,22] Meanwhile, with the capability of characterizing local bonding and coordination environment, Raman spectroscopy has been used to study aqueous uranyl species since this technique is also capable of monitoring progression of ongoing reactions quantitatively.[7,23−28] Thus, by coupling Raman with SAXS as our spectroscopic probes, utilizing carefully purified uranyl nitrate as starting material and controlled addition of simple transition metal salts as catalysts, the self-assembly reaction rate of the uranyl cluster U_{24} could be tuned.

EXPERIMENTAL SECTION

Caution! *Although isotopically depleted uranium was used in this study, precautions for handling toxic and radioactive materials should be followed.*

Uranyl nitrate was obtained from Fluka and recrystallized from hot water prior to use. All other chemicals were used as received. Powder XRD patterns were recorded on a Rigaku Ultima IV diffractometer using Cu Kα radiation of 0.15418 nm. Raman spectra were recorded on a Thermo Scientific DXR spectrometer with a 760 nm laser source. Small-angle X-ray scattering (SAXS) was recorded on an Anton Paar's SAXSess unit with Cu Kα radiation of 0.15418 nm. Data were further analyzed with the IRENA Package[29] of IGOR Pro.

Lithium uranyl trioxide monomers $[Li_4(UO_2)(O_2)_3{\cdot}4H_2O]$ were synthesized as previously reported.[8,20] In a beaker, 0.5 g of uranyl nitrate was dissolved in 6 mL of water and cooled to ~2 °C in an ice–water bath. In two separate vials, 3 mL of 4 M LiOH and 3 mL of 30% H_2O_2 solutions were also cooled to ~2 °C. Then LiOH and H_2O_2 solutions were combined while stirring (in an ice–water bath), followed by addition of uranyl nitrate solution resulting in a bright orange solution. To that solution was added 30 mL of cold ethanol with continuous stirring. The bright yellow precipitate was recovered by vacuum filtration and washed several times with cold ethanol and dried in air. After drying, 0.34 g of yellow solid was recovered, with a yield of 75% based on uranium. Powder XRD revealed a cubic phase as reported previously[8] (Figure SI1, Supporting Information).

Cluster self-assembly experiments were conducted in 4 mL glass vials. For a typical experimental run, uranyl trioxide monomer (14.5 mg) was dissolved in 0.5 mL of water or catalyst solution of various concentrations to make a 0.1 M monomer solution. The vial was then monitored with Raman at 23–25 °C. Simultaneously, at desired intervals, 20 μL of solution was sampled and diluted to 180 μL of water, filtered through a 0.22 μm syringe filter, and sealed in a 1.5 mm diameter glass capillary for SAXS evaluation. Small-angle X-ray scattering data were collected on an Anton Paar SAXSess instrument utilizing Cu Kα radiation (1.54 Å) and line collimation. Solutions were measured in 1.5 mm glass capillaries. Pure water was used for the background, and scattering was typically measured for 20–30 min. SAXSQUANT software was used for data collection, treatment, and preliminary analysis (normalization, primary beam removal, background subtraction, desmearing, and smoothing to remove extra noise created by the desmearing routine and Guinier analysis to determine R_g and I_0). The core–shell fits of the scattering data were carried out utilizing Modeling II in the IRENA[29] macros within IGOR Pro. U_{28} clusters synthesized prior[7] were used for Raman characterization. Simulated scattering curves and the radius of gyration (R_g) for the full U_{24} capsule and the square subunit were calculated from the single-crystal X-ray structure using SolX.[30]

RESULTS AND DISCUSSION

Two distinct Raman signals render easy monitoring of the growth of U_{24} over a period of time. The Raman peak at 810 cm^{-1} is attributed to O≡U≡O (henceforth referred to as the "*yl*") for the monomer, cluster, and any intermediate species, while the broad peak at 710–722 cm^{-1} is contributed by the terminal peroxide ligand of the monomer or reactant intermediates, discussed below. The latter also represents the concentration of reactant or intermediate material of this U_{24} self-assembly reaction. The smaller peak at 840 cm^{-1} with overlap from the yl oxygen peak falls within a complicated region for the uranyl system. Both solid and solution state Raman spectrum of Li-monomer and solid Li–U_{24} crystals are also plotted for comparison in Figure 1. Previous studies of uranyl hydroxide minerals and other aqueous species indicate that the peak at 840 cm^{-1} that is dominant in the U_{24} solution and solid spectra could be the stretching of a bridging peroxide between uranium centers.[23,25] Recent calculations and experiments also suggested this peak coincides with the bridging peroxide species found in uranyl–peroxide clusters[27] and studtite.[31] It is to be noted that the monomer peaks are observed at 838–842 cm^{-1}, while U_{24} mother liquor and U_{24} crystals display peaks at 844 and 848 cm^{-1}, respectively. This

dx.doi.org/10.1021/ic501587g | Inorg. Chem. 2014, 53, 10506–10513

indicates the complex nature of the Raman response in this region. The origin of the 838 cm^{-1} peak for the monomer might be a small amount of U_{24} or some other oligomeric impurity, as it can be present in different concentrations in different batches of starting materials. However, since the 844 cm^{-1} peak is the most distinct feature of U_{24} compared to the U_{28} cluster[7] (as U_{28} has bridging peroxide ligands only and no bridging hydroxyl ligands, Figure 2) it could be assigned to

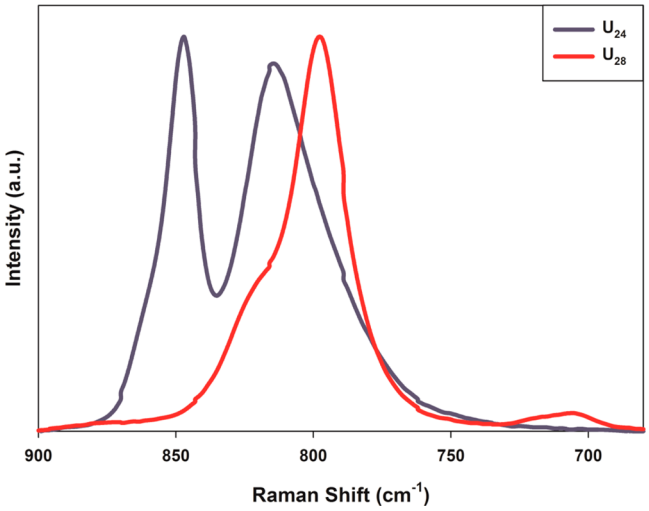

Figure 2. Normalized spectrum of U_{24} $[UO_2(O_2)(OH)]_{24}^{24-}$ (blue) and U_{28} $[UO_2(O_2)_{1.5}]^{28-}$ (red) in the solid state. Both uranyl clusters exhibit the prominent O≡U≡O peak at lower frequency. The second distinct peak for U_{24} we attribute to the OH ligand, as its presence is the major difference between U_{24} and U_{28}. The shoulder of the U_{28} O≡U≡O peak we attribute to the encapsulated uranyl species, as this peak shifts as a function of different encapsulated species; see Figure SI3, Supporting Information.

bridging hydroxyl groups connecting four-membered rings within the U_{24} structure. Also, a recent paper by McGrail et al. reports a new Raman peak at 878 cm^{-1} which we do not observe for U_{24} synthesized from uranyl nitrate purchased from Fluka, even if used as received, in multiple repeated syntheses.[28] On the other hand, when uranyl nitrate procured from SPI chemicals was used as received, we did observe the peak at 878 cm^{-1}, and hence, we attribute it to impurities present in the starting material which seems difficult to eliminate.

Nevertheless, despite the ambiguity of this 844 cm^{-1} peak, which is beyond the scope of this paper, it is still reasonable to associate U_{24} product formation to the growth of this peak, and we henceforth use it to monitor the formation process of U_{24} in solution. The *yl* oxygen (O≡U≡O) peak around 810 cm^{-1} was used as an internal standard to eliminate instrument deviation over time even though a slight change in intensity and position was observed. The spectra of the monomer, both in the solid and in the solution state, matched well enough to indicate that the monomer species retained its original structure when freshly dissolved, despite very slight shifting of the *yl* oxygen peak. The shift could be attributed to the difference in coordination environment in the solid state versus aqueous solution, based on association with water and alkali cations. Continuous monitoring of Li monomer for 4 days revealed no significant change in the spectrum. Thus, indicating that without any added catalyst, the self-assembly reaction rate is extremely slow if not nonreactive (Figure 3).

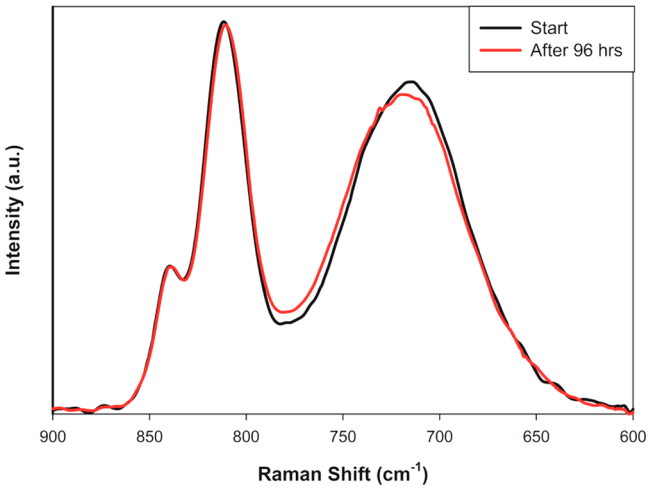

Figure 3. Raman spectra of 0.1 M Li monomer aqueous solution: newly dissolved (black) and after 4 days at room temperature (red).

All spectra displayed in Figure 1 discussed below are normalized to the *yl* oxygen peak area for better comparison of peroxo and hydroxyl peaks as well as to evaluate the relative area of other peaks.[32] While monitoring reactions by Raman, addition of 100 μM transition metal or halogen salt yielded no new peaks. Salts of $Ni(NO_3)_2$, $Cr(NO_3)_2$, and KIO_3 had no impact on the monomer to cluster conversion. However, $Cu(NO_3)_2$ and $Co(NO_3)_2$ both accelerated the reaction significantly, polymerizing monomers into U_{24} clusters in approximately 30 h (Figure 4a–c). Comparing copper and cobalt salts, the reaction rate for cobalt was slightly faster than the copper salt but the product yield for cobalt was significantly lower compared to copper possibly due to side reactions (Figure 4c).

After initial screening, Cu^{2+} was selected as the ideal candidate to proceed with detailed experiments since it produced the highest yield of U_{24} capsules and displayed higher catalytic activity. Thereafter, we conducted a series of experiments to determine suitable conditions to monitor formation of U_{24} clusters (Figure 5). Reactivity of Cu^{2+} is tested to be effective from 10 μM to 1 mM or 0.01% to 1% of uranyl concentration. At 10 μM concentration, the reaction takes several days to complete and therefore was deemed to be time consuming to follow, whereas at 1.0 mM the reaction rate was too fast to monitor effectively. Hence, after optimizing the reaction conditions, 100 μM Cu^{2+} was found to be ideal for studying this reaction mechanism efficiently and effectively. We also noted that if significantly more than a catalytic amount of transition metal salt is added, a precipitate is formed almost immediately with effervescence, indicating decomposition of peroxide. At such high alkaline condition, most likely copper produces copper hydroxide precipitates[33] or associates and precipitates with highly negatively charged ions such as $[(UO_2)(O_2)]^{4-}$ or U_{24} in solution or even plausibly form nanoparticles.[34]

During the reaction we noticed a shift in the uranyl-bound peroxide peak. Initially, the peroxide peak shifts slightly to higher wave numbers as it starts to diminish over time, which is not observed for nonreactive samples, indicating formation of intermediate species (Figure 4b).

Furthermore, the increase of the U_{24} hydroxyl peak lags consumption of terminal peroxide species, also suggesting formation of an intermediate. This is another indication of the

dx.doi.org/10.1021/ic501587g | Inorg. Chem. 2014, 53, 10506–10513

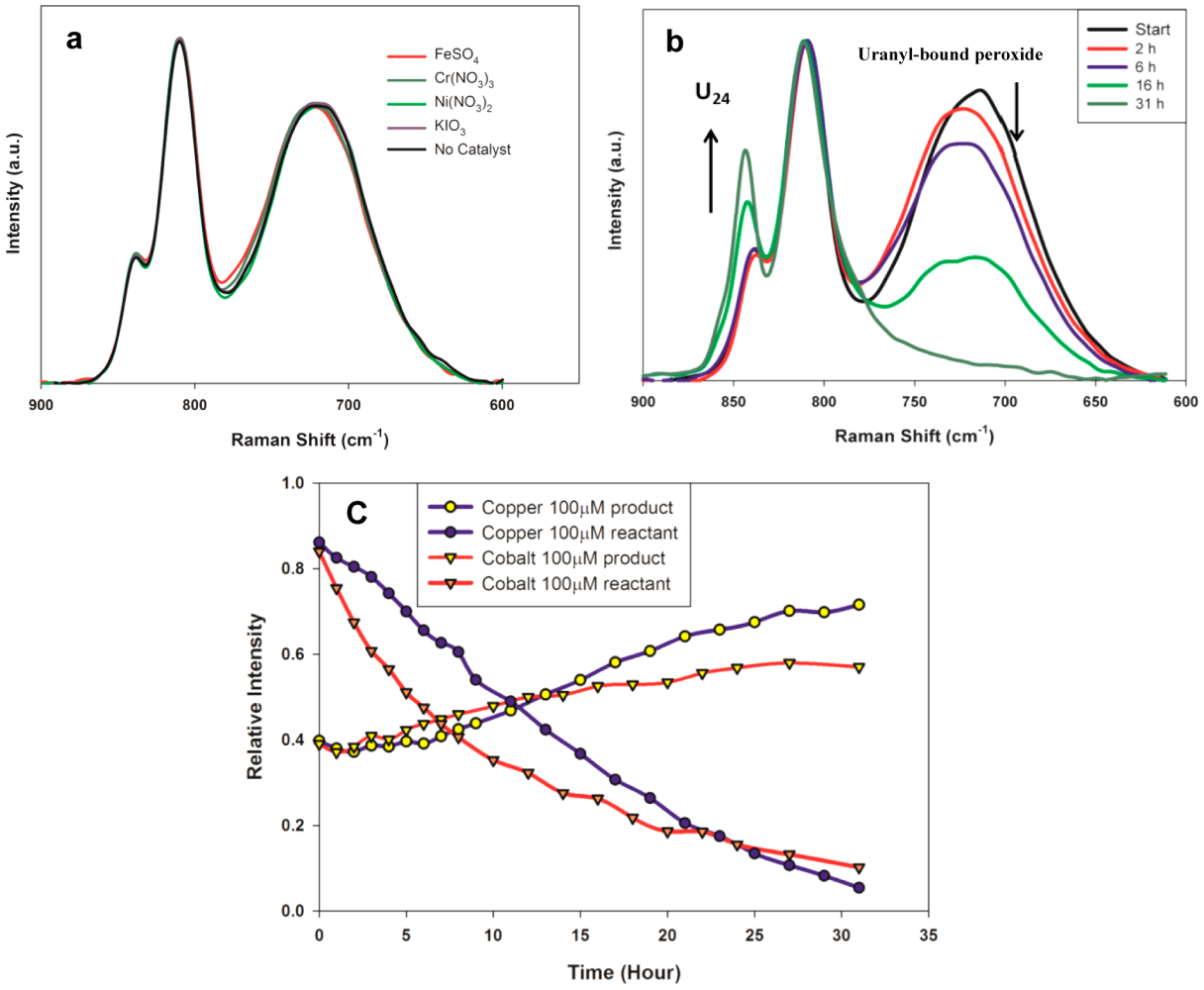

Figure 4. Raman evolution of 0.1 M Li monomer solution with 100 μM $Ni(NO_3)_2$, $FeSO_4$, $Cr(NO_3)_3$, and KIO_3 after 96 h (a), 100 μM $Cu(NO_3)_2$ (b), and relative peak intensity vs reaction time plots with the presence of 100 μM $Cu(NO_3)_2$ and $Co(NO_3)_2$ (c). Reactant (terminal peroxide) and product (hydroxyl) peaks are represented by their relative intensity against the O≡U≡O peak.

complicated nature of uranyl−peroxide cluster formation. While the peroxide peak starts to decrease from the beginning of the reaction, the hydroxyl peak does not show a significant increase until well into the reaction progress. Closer scrutiny suggests, with some deviation, the bridging hydroxyl peak starts to grow significantly after about one-third of the peroxide peak is consumed. This observation is in agreement with the proposed mechanism as illustrated in Scheme 1. Initially, four uranyl−peroxide monomers form a four-membered ring, which is the sub-building unit of U_{24} clusters. The result is a loss of 4 peroxide ligands out of a total of 12 peroxide ligands. Once the four-membered rings are established, further displacement of peroxide species on the outer sphere by the hydroxyl groups results in a decrease of the peroxide peak and an increase of the hydroxyl peak at 843 cm^{-1} simultaneously, resulting in formation of U_{24} clusters. Given these observations, it is necessary to classify the terminal peroxo peak as representing monomer and intermediate species (presumably tetramers as shown in Scheme 1). We expect the peroxide ligands of these putative tetramer species to be fluxional and highly reactive, as the tetramer has never been isolated. If heating or a slight excess of catalysts is used, controlled loss of peroxide ligand is hampered and results in a hydroxide precipitate. Also, as the U_{24} cluster forms, the base of the O≡U≡O peak becomes slightly broad (775 cm^{-1}) compared to the monomer peak. From a structural point of view, the inherently bent uranyl peroxide dimer[13,14] translates to ring curvature via templating the Li^+ cation inside the capsule. Observation of this tetramer intermediate is explored further below via small-angle X-ray scattering (SAXS).

Initially, no significant scattering was observed by SAXS (Figure 6), which is in agreement with Raman observations. In the reaction window of the first few hours, in which there is a minimal increase of the hydroxyl peak but a significant decrease of uranyl-bound peroxide species, X-ray scattering analyses presented interesting results. (N.B.: We need to consider these result with some caution, given the low concentration and the small size of the scattering species.) Since U_{24} has 6 times the electrons and a much larger R_g than the four-membered ring (tetramer), even a small amount of U_{24} (calculated R_g [radius of gyration] = 6.467 Å) easily overwhelms the scattering from the smaller tetramers (calculated R_g = 3.334 Å). This is because the scattering intensity scales by r^6 and Z^2 (Z = atomic number) according to the equation $I_1(q) = I_0\rho_1{}^2V_1{}^2P(q)$, where $P(q)$ is the form factor of the scatterer, V is the volume, ρ is the electron density, I_1 is the total scattered intensity, and I_0 is the scattered intensity of a single electron.[35]

dx.doi.org/10.1021/ic501587g | Inorg. Chem. 2014, 53, 10506−10513

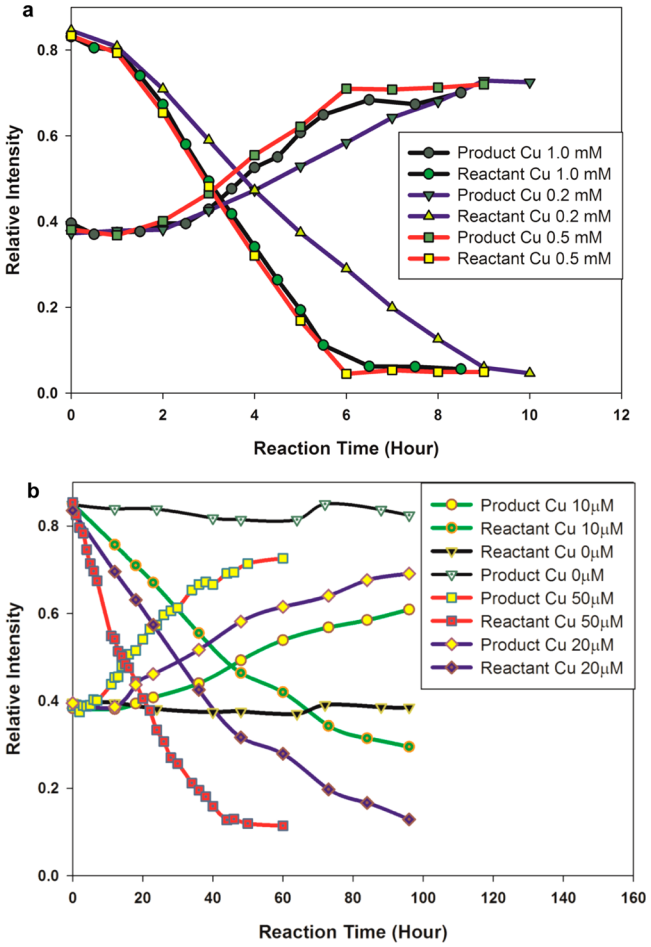

Figure 5. Relative peak intensity evolution for 0.1 M Li monomer solution over time with the presence of 1.0, 5×10^{-1}, and 2.0×10^{-1} mM $Cu(NO_3)_2$ (a) and 50, 20, 10, and 0.0 μM $Cu(NO_3)_2$ (b). Peroxo and hydroxyl peaks are represented by their relative intensity against the O≡U≡O peak.

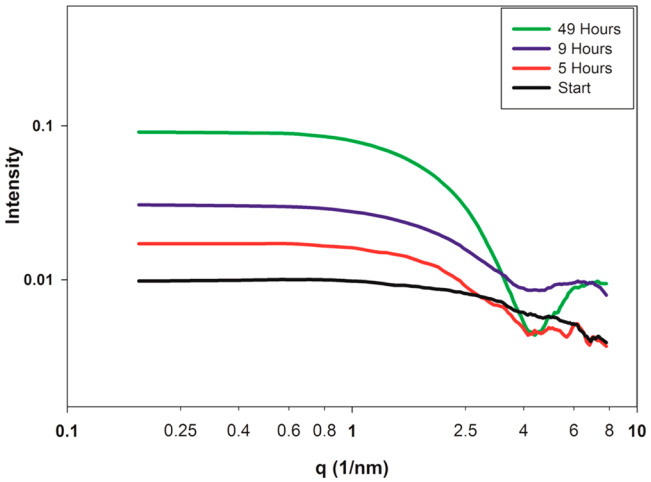

Figure 6. SAXS scattering curve following the evolution of 0.1 M Li monomer solution with 1×10^{-1} mM $Cu(NO_3)_2$ with time.

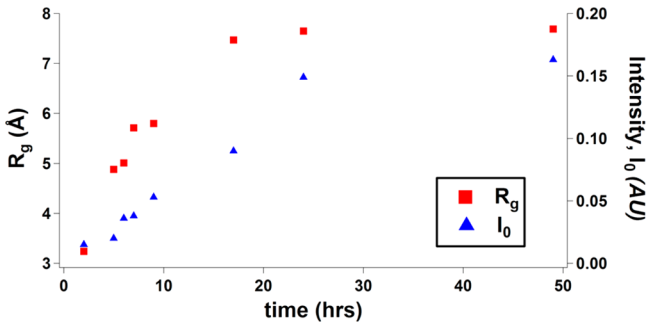

Figure 7. Radius of gyration (R_g) and zero-angle scattering intensity (I_0) of small-angle X-ray scattering data plotted as a function of time for the evolution of 0.1 M Li monomer solution with 1×10^{-1} mM $Cu(NO_3)_2$.

Figure 6 shows some select scattering curves, and Figure 7 shows a plot of the R_g and I_0 (zero angle scattering intensity, consistent with concentration of scatterers) as a function of time for a 48 h monitored experiment of the transition for the Li monomer to Li–U_{24}, determined by the Guinier approximation.[35] There is an increase in both R_g and I_0, which levels off in approximately 24 h. This indicates an increase in both the average size and the concentration of scattering species. At 2 h, R_g = 3.24 Å corresponds with the U_4 tetrameric building block of U_{24}. From 6 to 10 h, R_g increasing from 5 to 6 Å represents a mixture of U_{24} plus U_4 tetramer. The rise above 7 Å may suggest some aggregation of U_{24} with U_4 tetramers rings, similar to the case observed for U_{120}, a core cluster[36] with associated pentagonal rings outside the capsule.

Using SolX,[30] we also fit the simulated scattering data of Li–U_{24} with a core–shell model using Modeling II in Irena,[29] and these parameters that describe the U_{24} capsule along with those

Scheme 1. Proposed U_{24} Self-Assembly Reaction Mechanism with Four-Membered Rings (tetramer) as a Possible Intermediate

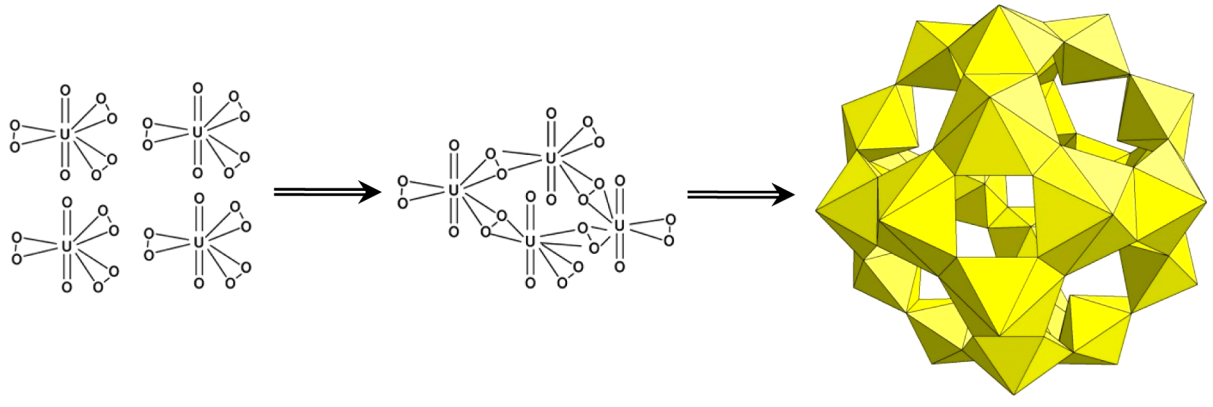

dx.doi.org/10.1021/ic501587g | Inorg. Chem. 2014, 53, 10506–10513

for the experimental data of the reaction solution at 9, 24, and 49 h are compiled in Table 1; see also Figures SI4 and SI5,

Table 1. Core-Shell Fit of Simulated and Experimental X-ray Scattering Data for U_{24}

experimental[a]	shell thickness (Å)	core radius (Å)	total diameter (Å)	core ρ^b	shell ρ^b
simulated	2.2	5.1	14.6	1.44	119
9 h reaction	1.0	6.0	14.0	fixed to match the simulated data	
24 h reaction	1.8	5.9	15.4		
49 h reaction	3.3	5.0	16.6		

[a]See also Figures SI4 and SI5, Supporting Information. [b]X-ray scattering length density (10^{10} cm^{-2}) relative to fixed solvent ρ = 10 for water.

Supporting Information. For the simulated scattering data, the structural (core diameter and shell thickness) and electron density (ρ) parameters were freely refined against a fixed solvent density (water, $\rho = 10^{10}$ cm^{-2}). From this we obtained an electron density of the core that is considerably less than that of bulk water, and the uranium-containing shell that has an electron density ~12 times greater than bulk water. These are reasonable results, given the core contains only structured Li^+ and water molecules, and the high scattering from uranium is self-evident. The core and shell dimensions also agree well with that of the X-ray structure. These density values were then fixed for fitting the experimental data, and the core radius and shell thickness were freely refined against these. Consistent with the increasing R_g (Figure 7), the total diameter of the cluster species increased with reaction time. We also observe a steady increase in the shell thickness with increasing time. This could also be consistent with tetramer intermediates associating with the U_{24} capsule, as described above. The core radius and related electron density results should be treated cautiously, however, as we know from prior studies[9,37] that the contents of the core are extremely dynamic and the solid-state structure provides only one possible snapshot. In summary, SAXS data revealed that (1) the tetramer building blocks dominate the reaction solution the first 4 h (agreeing with Raman data of Figure 5a) and (2) U_{24} growth accelerates after tetramers are formed. In addition, SAXS data revealed the possible persistence of the tetrameter rings, associating with U_{24} capsules, even as U_{24} species become dominant with increased reaction time.

To further investigate the effect of free peroxide on the reaction rate, 10 μL of 30% H_2O_2 was added to already complete reaction solution, and the free peroxide peak appeared almost immediately at 872 cm^{-1} (Figure 8a). An increase of the uranyl-bound peroxide peak at 730 cm^{-1} was immediately observed, indicating a back reaction that converts U_{24} to the monomer and other intermediates, since the 844 cm^{-1} hydroxyl peak decreased as well. The diminution of the 872 cm^{-1} peak over time clearly indicates decomposition of free H_2O_2. Simultaneously, the hydroxyl peak intensity reverts back to the original concentration level of the original monomer solution. After about 7 h, as expected, the peak around 730 cm^{-1} starts to shift slightly toward lower wave numbers as opposed to forming U_{24} right away and reaches its maxima after all free peroxides were consumed, indicating only bound peroxide species remained in solution. Afterward, the hydroxyl peak starts to grow back and shifts to the original U_{24} solution peak, while the peak around 710 cm^{-1} (shifted from 730 cm^{-1})

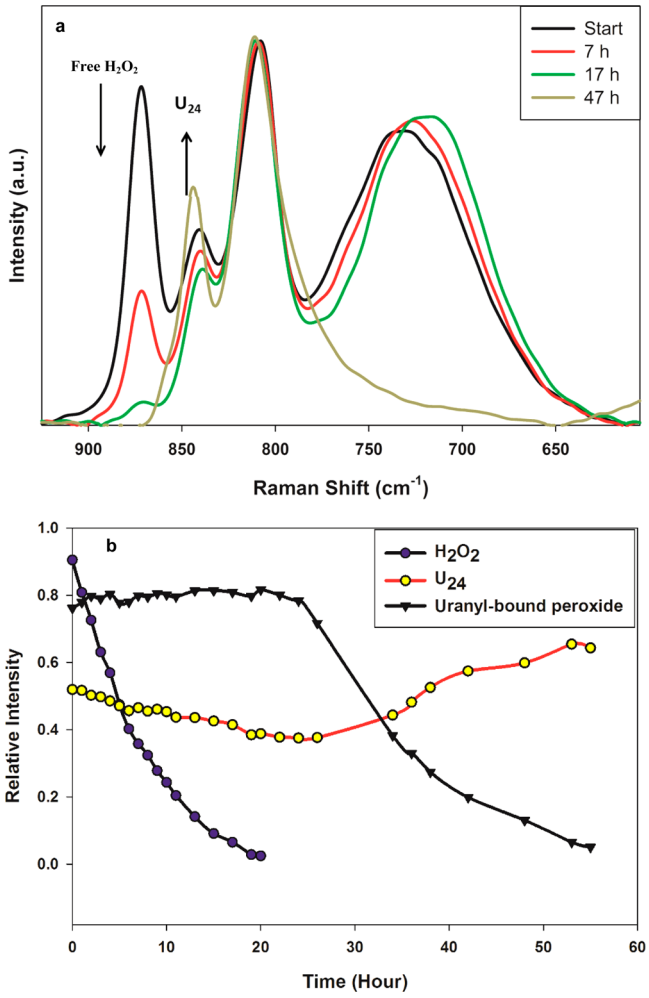

Figure 8. Raman evolution of 0.1 M Li monomer solution with 0.1 mM $Cu(NO_3)_2$ and additional H_2O_2 (a), and relative intensity against O≡U≡O evolution of H_2O_2, hydroxyl, and uranyl-bound peroxide peak (b) over time.

starts to decrease, repeating the behavior already observed for the monomer self-assembly reaction as described earlier. The final spectra depict the typical U_{24} spectrum. Figure 8b clearly indicates that product formation does not start until all the H_2O_2 has been decayed completely. As long as the H_2O_2 peak was persistent, decomposition of initial U_{24} was observed, as well as simultaneous growth of reactant materials. However, as soon as the peroxide peak coordinated to monomer species diminished, regrowth of the U_{24} peak was observed. In other words, the reaction is completely reversible and appears to follow the same pathway, from monomer to U_{24} and from U_{24} to monomer.

This result also indicates that reactive copper species form instantaneously with addition of peroxide, which only catalyzes decomposition of free and uranyl-bound peroxides present in solution, since it does not interfere with U_{24} formation once excess peroxides are consumed. This copper species reactivates again to destroy additional peroxide upon addition of fresh peroxide solution to an already completed reaction solution. This observation is consistent with an autocatalytic Fenton-like mechanism[34] and with self-poisoning behavior. However, regeneration of catalytic copper species with addition of fresh peroxide and the absence of brown precipitates (if a catalytic amount of copper is used) leads to ambiguous speculation

dx.doi.org/10.1021/ic501587g | Inorg. Chem. 2014, 53, 10506−10513

about the final form of the catalytic species once all the peroxide is decomposed. Furthermore, based on the findings of Chechik et al.,[34] it could be assumed that since copper scavenges for competing CO_3^{2-} ligand under alkaline condition it leads to fast formation and a higher yield of uranyl nanoclusters.

For comparison, the widely employed one-step self-assembly reaction from which uranyl−peroxide clusters were first assembled[1] was also monitored. To 0.1 mL of 0.5 M uranyl nitrate solution, 0.07 mL of 30% hydrogen peroxide was added, followed by addition of 0.1 mL of 2 M LiOH solution. Similar to the Li monomer system with additional hydrogen peroxide just described above, an intense free hydrogen peroxide peak was observed at 872 cm^{-1} as well as the typical O≡U≡O peak at 810 cm^{-1}. The peak around 700 cm^{-1} indicated formation of monomer-like species. After catalyst was added, the free hydrogen peroxide peak diminished over several hours, during which time a slight shift and increase of monomer peroxide peak was observed. The peak at around 840 cm^{-1} also followed the same trend as the monomer with H_2O_2 in solution that decreased as H_2O_2 decomposed. However, without a catalyst, even after all of the free hydrogen peroxide had decomposed, the spectrum showed little to no evolution over 5 days with no decrease of the 730 cm^{-1} peak or increase of the hydroxyl (U_{24}) peak, indicating a negligible reaction rate and essentially no formation of significant product after 6 days (Figure 9). This

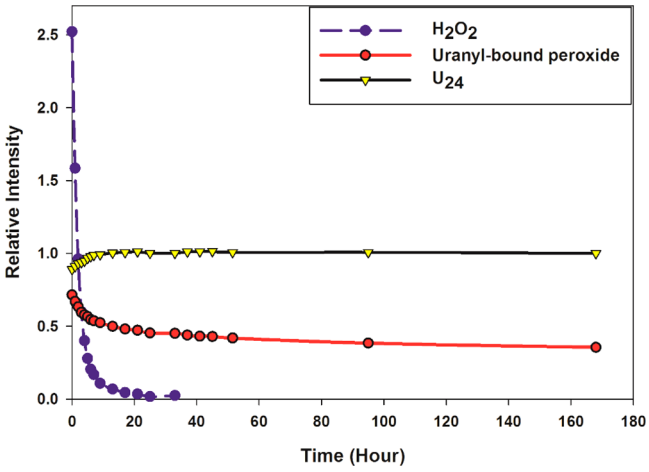

Figure 9. Relative intensity evolution of H_2O_2, uranyl-bound peroxide, and U_{24} capsule from monitoring the "one-pot" reaction (see text).

result is consistent with the following: (1) the monomer is indeed an intermediate to the clusters and (2) obtaining a substantial yield is not consistent over multiple syntheses using this method. The latter point suggests that the unintentional presence or absence of catalytic material that oxidizes peroxide to diatomic oxygen should be considered in performing these syntheses.

Finally, we discuss the mode of activity of the catalyst. All potential catalysts we tested were added in small enough quantities so that precipitation of hydroxides was not visually apparent in these conditions of high alkalinity, but formation of oxide nanoparticles cannot be entirely ruled out. UV−vis absorption techniques could not be employed since the strong absorption peak of U_{24} would mask any weak featureless shoulder of copper nanoparticles around 375 nm. On the other hand, as discussed above, formation of even a small concentration of nanoparticles (with radius > 1.8 nm size of U_{24}) would likely be detected by SAXS, and this was not the case. Discerning mechanisms can be complicated by the fact that peroxide can act as both an oxidizer and a reducing agent. Since Fe^{II}, Ni^{II}, and iodine had no effect on the monomer-to-cluster conversion, this suggests the reaction is better catalyzed by oxidation of the peroxide rather than reduction, as these ions do not reduce readily under the conditions of the experiment. Also, reaction with $KMnO_4$ as catalyst proceeds too fast; however, it does not result in clean U_{24} formation (data not shown). Although Fe^{II} is readily oxidized to Fe^{III} in alkaline conditions, Fe^{III} is not a strong oxidizer. Therefore, this reaction would have no turnover cycles once all the Fe^{II} is oxidized. Cr^{III} and Cr^{VI} are readily accessed in alkaline conditions, but they predominantly exist as stable oxoanions including $Cr(OH)_4^-$, CrO_4^{2-}, and $Cr_2O_7^{2-}$, so perhaps they cannot effectively complex and reduce or oxidize a peroxide ligand.[38] Co^{II}, on the other hand, is an effective catalyst for the reaction of study, but the monomer-to-cluster conversion never goes to completion with this catalyst, suggesting side reactions. This would be consistent with Co^{II} (via Co^{II} to Co^{III} oxidation) reducing and therefore splitting O_2^{2-} to oxo ligands, which could then readily coordinate and polymerize the uranyl monomer. On the other hand, copper readily complexes ligands such as peroxide and is known to easily cycle between Cu^{II} and Cu^{I}, especially in the presence of peroxide.[39] Reaction with $Cu^{II/I}$ as a catalyst is summarized as follows (see also Scheme 1)

$$24[UO_2(O_2)_3]^{4-} \xrightarrow{Cu^{II/I}} 6[UO_2(O_2)_2]_4^{8-} + 24O_2(g)$$

$$6[UO_2(O_2)_2]_4^{8-} + 24OH^- \xrightarrow{Cu^{II/I}} 6[UO_2(O_2)(OH)_2]_4^{8-} + 24O_2(g)$$

$$6[UO_2(O_2)(OH)_2]_4^{8-} \xrightarrow{(fast)} [UO_2(O_2)(OH)]_{24}^{24-} + 24OH^-$$

$$[UO_2(O_2)(OH)]_{24}^{24-} + 48H_2O_2 \rightarrow 24[UO_2(O_2)_3]^{4-} + 24H_2O + 72H^+$$

CONCLUSIONS

This study has provided insight into the self-assembly mechanism of uranyl peroxide capsule formation from monomeric species and the role of excess peroxide and added catalysts (redox active transition metals) on the reaction pathway and rate. When potential catalytic impurities are rigorously excluded, the self-assembly reaction rate is essentially turned off at room temperature and even reversed if excess peroxide is added to a solution containing only capsules. These results indicate there is a kinetic barrier to conversion of uranyl peroxide monomers to capsules and decomposition of peroxide ligands, such as by oxidation to O_2 gas, drives the reaction forward. This may also be accomplished with heat but offers less control as precipitation of uranyl hydroxides is often the end result. With this study we hope to bring forth further expansion of this class of nanomaterials, both by stimulating thought of new synthetic methods and compositions and by providing means of obtaining pure materials that are necessary for studies of chemical and electrochemical behavior of uranyl clusters in solution. Elimination of terminal peroxides to form

dx.doi.org/10.1021/ic501587g | Inorg. Chem. 2014, 53, 10506−10513

clusters is analogous to elimination of water in hydrolysis and condensation (olation) reactions to form metal−oxo clusters from monomers and metal oxide materials from incipient clusters, thus drawing another analogy to the transition metal polyoxometalates.

■ ASSOCIATED CONTENT

Supporting Information

XRD patterns, Raman spectra, SAXS results. This material is available free of charge via the Internet at http://pubs.acs.org.

■ AUTHOR INFORMATION

Corresponding Author

*E-mail: may.nyman@oregonstate.edu.

Notes

The authors declare no competing financial interest.

■ ACKNOWLEDGMENTS

The reported synthesis and catalysis study was supported as part of the Materials Science of Actinides, an Energy Frontier Research Center funded by the Department of Energy, Office of Science and Office of Basic Energy Sciences under award number DE-SC0001089.

■ REFERENCES

(1) Burns, P. C.; Kubatko, K.-A.; Sigmon, G.; Fryer, B. J.; Gagnon, J. E.; Antonio, M. R.; Soderholm, L. *Angew. Chem., Int. Ed.* **2005**, *44*, 2135−2139.
(2) Qiu, J.; Burns, P. C. *Chem. Rev.* **2013**, *113*, 1097−1120.
(3) Burns, P. C. *C. R. Chim.* **2010**, *13*, 737−746.
(4) Nyman, M.; Burns, P. C. *Chem. Soc. Rev.* **2012**, *41*, 7354−7367.
(5) Unruh, D. K.; Burtner, A.; Pressprich, L.; Sigmon, G. E.; Burns, P. C. *Dalton Trans.* **2010**, *39*, 5807.
(6) Li, Y.; Burns, P. C. *J. Solid State Chem.* **2002**, *166*, 219−228.
(7) Nyman, M.; Rodriguez, M. A.; Alam, T. M. *Eur. J. Inorg. Chem.* **2011**, *2011*, 2197−2205.
(8) Nyman, M.; Rodriguez, M. A.; Campana, C. F. *Inorg. Chem.* **2010**, *49*, 7748−7755.
(9) Nyman, M.; Alam, T. M. *J. Am. Chem. Soc.* **2012**, *134*, 20131−20138.
(10) Alcock, N. W. *J. Chem. Soc. A: Inorg., Phys., Theor.* **1968**, 1588−1594.
(11) Kubatko, K.-A.; Forbes, T. Z.; Klingensmith, A. L.; Burns, P. C. *Inorg. Chem.* **2007**, *46*, 3657−3662.
(12) Gil, A.; Karhanek, D.; Miro, P.; Antonio, M. R.; Nyman, M.; Bo, C. *Chem.—Eur. J.* **2012**, *18*, 8340−8346.
(13) Miro, P.; Pierrefixe, S.; Gicquel, M.; Gil, A.; Bo, C. *J. Am. Chem. Soc.* **2010**, *132*, 17787−17794.
(14) Vlaisavljevich, B.; Gagliardi, L.; Burns, P. C. *J. Am. Chem. Soc.* **2010**, *132*, 14503−14508.
(15) Wylie, E. M.; Peruski, K. M.; Weidman, J. L.; Phillip, W. A.; Burns, P. C. *ACS Appl. Mater. Interfaces* **2014**, *6*, 473−479.
(16) Burns, P. C.; Hughes, K.-A. *Am. Mineral.* **2003**, *88*, 1165−1168.
(17) McNamara, B. K.; Buck, E. C.; Hanson, B. D. Observation of Studtite and Metastudtite on Spent Fuel; In *Scientific Basis for Nuclear Waste Management XXVI; Materials Research Society Symposium Proceedings*; Materials Research Society, Warrendale, PA: 2003; Vol. *757*, pp 401−406.
(18) Burakov, B. E.; Strykanova, E. E.; Anderson, E. B. *MRS Proceedings* **1996**, *465*, 1309−1311.
(19) Nyman, M.; Alam, T. M. *J. Am. Chem. Soc.* **2012**, *134*, 20131−20138.
(20) Armstrong, C. R.; Nyman, M.; Shvareva, T.; Sigmon, G. E.; Burns, P. C.; Navrotsky, A. *Proc. Natl. Acad. Sci. U.S.A.* **2012**, *109*, 1874−1877.
(21) Qiu, J.; Ling, J.; Sui, A.; Szymanowski, J. E. S.; Simonetti, A.; Burns, P. C. *J. Am. Chem. Soc.* **2012**, *134*, 1810−1816.
(22) Qiu, J.; Nguyen, K.; Jouffret, L.; Szymanowski, J. E. S.; Burns, P. C. *Inorg. Chem.* **2013**, *52*, 337−345.
(23) Toth, L.; Begun, G. *J. Phys. Chem.* **1981**, *85*, 547−549.
(24) Nguyen-Trung, C.; Palmer, D. A.; Begun, G. M.; Peiffert, C.; Mesmer, R. E. *J. Solution Chem.* **2000**, *29*, 101−129.
(25) Faulques, E.; Russo, R.; Perry, D. *Spectrochim. Acta Part a: Mol. Biomol. Spectrosc.* **1994**, *50*, 757−763.
(26) Tsushima, S.; Nagasaki, S.; Tanaka, S.; Suzuki, A. *J. Phys. Chem. B* **1998**, *102*, 9029−9032.
(27) Bastians, S.; Crump, G.; Griffith, W. P.; Withnall, R. *J. Raman Spectrosc.* **2004**, *35*, 726−731.
(28) McGrail, B. T.; Sigmon, G. E.; Jouffret, L. J.; Andrews, C. R.; Burns, P. C. *Inorg. Chem.* **2014**, *53*, 1562−1569.
(29) Ilavsky, J.; Jemian, P. R. *J. Appl. Crystallogr.* **2009**, *42*, 347−353.
(30) Tiede, D. M.; Zhang, R.; Chen, L. X.; Yu, L.; Lindsey, J. S. *J. Am. Chem. Soc.* **2004**, *126*, 14054−14062.
(31) Mallon, C.; Walshe, A.; Forster, R. J.; Keyes, T. E.; Baker, R. J. *Inorg. Chem.* **2012**, *51*, 8509−8515.
(32) The multiply bonded *yl* oxygen is extremely stable and does not chemically alter under the conditions of these experiments. The only way to alter this O≡U≡O species is via reduction of U^{6+} to U^{5+} or U^{4+}, which is also indicated by a distinct color change (i.e., to colorless and black or green, respectively), and this is also not observed nor is it expected in the reaction conditions under investigation. Therefore, this *yl* oxygen peak can serve quantitatively as an internal standard of total uranyl present in solution. Additionally, to further confirm that the *yl* peak is an additive combination of monomer plus U_{24} (plus intermediate species such as the tetramer), we combined pure monomer plus pure U_{24} in solution and characterized this solution by Raman spectroscopy (see Supporting Information for details.)
(33) Lee, H.; Lee, H.-J.; Sedlak, D. L.; Lee, C. *Chemosphere* **2013**, *92*, 652−658.
(34) Naqvi, K. R.; Marsh, J.; Chechik, V. *Dalton Transactions* **2014**, *43*, 4745−4751.
(35) Guinier, A.; Fournet, G. *Small-Angle Scattering of X-rays*; Wiley: New York, 1955.
(36) Ling, J.; Qiu, J.; Burns, P. C. *Inorg. Chem.* **2012**, *51*, 2403−2408.
(37) Alam, T. M.; Liao, Z.; Zakharov, L. N.; Nyman, M. *Chem.—Eur. J.* **2014**, *20*, 8302−8307.
(38) Baes, C. F.; Mesmer, R. E. *The Hydrolysis of Cations*; A Wiley-Interscience Publication: New York, 1976.
(39) Pham, A. N.; Xing, G. W.; Miller, C. J.; Waite, T. D. *J. Catal.* **2013**, *301*, 54−64.